

Alya: Towards Exascale for Engineering Simulation Codes

Mariano Vázquez^{1,2}, Guillaume Houzeaux¹, Seid Koric³, Antoni Artigues¹,
Jazmin Aguado-Sierra¹, Ruth Arís¹, Daniel Mira¹, Hadrien Calmet¹,
Fernando Cucchietti¹, Herbert Owen¹, Ahmed Taha³, and José María Cela¹

¹Barcelona Supercomputing Center BSC-CNS, Spain

²IIIA-CSIC, Spain

³National Center for Supercomputing Applications-NCSA, University of
Illinois at Urbana-Champaign, USA

Contact: mariano.vazquez@bsc.es , guillaume.houzeaux@bsc.es ,
koric@illinois.edu

Paper submitted to International Supercomputing Conference 2014

October 16, 2018

Abstract

Alya is the BSC in-house HPC-based multi-physics simulation code. It is designed from scratch to run efficiently in parallel supercomputers, solving coupled problems. The target domain is engineering, with all its particular features: complex geometries and unstructured meshes, coupled multi-physics with exotic coupling schemes and Physical models, ill-posed problems, flexibility needs for rapidly including new models, etc. Since its conception in 2004, Alya has shown scaling behaviour in an increasing number of cores. In this paper, we present its performance up to 100.000 cores in Blue Waters, the NCSA supercomputer. The selected tests are representative of the engineering world, all the problematic features included: incompressible flow in a human respiratory system, low Mach combustion problem in a kiln furnace and coupled electro-mechanical problem in a heart. We show scalability plots for all cases, discussing all the aspects of such kind of simulations, including solvers convergence.

1 Introduction

Alya (see for instance [1–5]) is a simulation code developed at Barcelona Supercomputing Center (BSC-CNS) since 2004, whose main architects are authors GH and MV. Alya is not a single-physics born sequential code, parallelized afterwards. On the other hand, it was designed from scratch as a multi-physics parallel code. It's main features are the following:

- It solves discretized partial differential equations (PDEs), preferring variational methods (particularly Finite Elements).

- Space discretization is based on unstructured meshes, with several types of elements (hexaedra, tetraedra, prisms, pyramids... linear, quadratic...) implemented.
- Both explicit and implicit time advance schemes are programmed.
- Depending on the case, staggered or monolithic schemes are programmed. However, staggered schemes with coupling iterations are preferred for large multi-physics problems.
- Parallelization is based on mesh partitioning (for instance using Metis [6]) and MPI tasks, which is specially well-suited for distributed memory machines. On top of that, some heavy weight loops are parallelized using OpenMP threads. Both layers can be used at the same time in a hybrid scheme.
- Alya sparse linear algebra solvers are specifically developed, with a tight integration with the overall parallelization scheme. There are no third-parties solver libraries required.
- Alya includes some geometrical tools which operate on the meshes for smoothing, domain decomposition or mesh sub-division. In particular, the latter is a key tool for large-scale simulations [7].

This paper addresses the performance of Alya in supercomputers, running up to 100K cores in Blue Waters, the sustained peta-scale system [8] hosted at the University of Illinois' National Center for Supercomputing Applications (NCSA). Blue Waters consists of traditional Cray XE6 compute nodes and accelerated XK7 compute nodes in a single Gemini interconnection fabric. Only XE6 nodes were used in this work, with each node containing two AMD Interlagos processors which totals to 16 floating point cores/XE6 node (NCSA, USA). Performance is measured through scalability when simulating coupled multi-physics problems in complex geometries coming from different domains. The selected cases are incompressible flow in the respiratory system, turbulent low Mach incompressible flows with combustion in a kiln furnace and non-linear solid mechanics coupled with electro-physiology in a human heart.

2 Alya general view

Alya is organized in a modular way: *kernel*, *services* and *modules*, which can be separately compiled and linked. Each *module* represents a different set of Partial Differential Equations (PDE), i.e. each module is a *physics*. To solve a coupled multi-physics problem, all the required modules are active and interacting following a certain workflow. Alya's *kernel* controls the run (it contains the solvers), the input-output and everything related to the mesh and geometry. With kernel and modules, a given Physical problem can be completely solved. The *services* are supplementary stuff, notably the parallelization service. Kernel, modules and services have well-defined interfaces and connection points.

2.1 Computational Mechanics Equations: the theoretical setup

Generally speaking, Alya deals with Computational Mechanics problems that can be modelled through conservation laws expressed as a set of partial differential equations:

$$\partial_t^* \Phi^\alpha = \partial_{x_i} F_i^\alpha = \partial_{x_i} C_i^\alpha + \partial_{x_i} K_i^\alpha$$

where Φ^α is the α -equation of the set. F_i^α is the compact notation of the fluxes for each of the equations, being divided in two terms, C_i^α and K_i^α , for convenience. The temporal derivative $\partial_t^* \Phi^\alpha$ is starred to note that it can be of first (like in fluid flows or excitable media) or second order (like in solid mechanics or acoustics). Subindices run through the space dimension of the space domain Ω . To these equations, boundary and initial conditions must be added depending on the problem under study.

The variational form is obtained by projection on a space W with its usual properties, where $\forall \Psi \in W$ after integration by parts of some of the fluxes (those labelled with K) yields, we obtain

$$\begin{aligned} \partial_t^* \int \Psi^\alpha \Phi^\alpha d\Omega = & \int \Psi^\alpha \partial_{x_i} C_i^\alpha d\Omega - \int \partial_{x_i} \Psi^\alpha K_i^\alpha d\Omega \\ & + \int \Psi^\alpha K_i^\alpha n_i d\partial\Omega. \end{aligned} \quad (1)$$

The last of the right hand side terms can be used for imposing Neumann-like boundary conditions on the fluxes themselves, being $\partial\Omega$ the domain boundary and n_i its exterior normal vector. The interpolation space where the variational form solution is to be found is (practically) the same as W , explicitly time independent. For that reason, the time derivative has been taken out of the space integral, with the additional hypothesis that Ω is not changing with time. These equations govern problems in fluid mechanics, solid mechanics, chemical reactions, quantum mechanics, heat transfer, etc.

In Alya, the method used to discretize in space the weak form Equation 1 is the finite element method. For the cases that additional numerical stabilization is required, we usually follow the the so-called Variational MultiScale method (see for instance [9]). Time is discretized using finite differences to obtain either explicit or implicit schemes of different orders. Time and space discretization of the weak form leads to a $\mathbf{A}\mathbf{u} = \mathbf{b}$ algebraic system.

The equations terms contain all the “physics” of a given problem. The governing equations are discretized in time and space in a certain way and programmed in a module. So the module main task is to compute the elementary matrix and right-hand-side of its corresponding set of equations, including all the numerical subtleties, boundary conditions, material models and so on. These matrices are assembled in a global matrix and a global right-hand-side vector, creating an algebraic system.

These algebraic systems can be very large. In Alya, we prefer to solve them using iterative methods which are very well suited for parallel programming. According to the problem solved, we follow a wide range of iterative strategies. On one hand, the explicit schemes, which can be viewed as the most simple iterative method with a unique simple (Richardson) iteration per time step. On the other hand lie schemes such as GMRES, BiCGSTAB, CG [10] or Deflated CG [11,12]. Both explicit and implicit schemes are illustrated in Figure 1. Apart from the time loop, a linearization loop may be necessary for non-linear problems when using the implicit scheme.

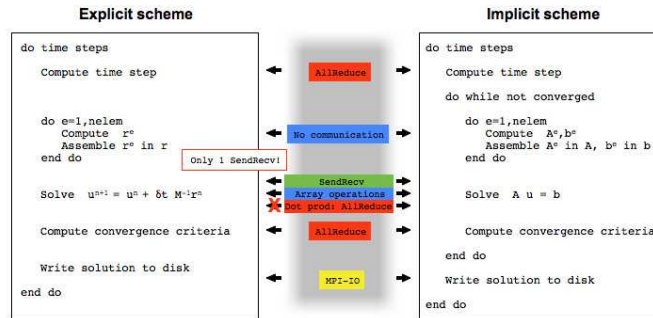


Figure 1: Typical explicit and implicit schemes

2.1.1 Coupling schemes

In Alya, Multi-physics problems are simulated through coupling modules. Although the code structure allows much more complex situations, in this paper we focus in a certain kind of coupling, where all happens on the same domain and domain discretization. In these cases, the main features are:

- All problems are solved on the same mesh, no interpolation is required.
- The total number of degrees of freedom is equal to the number-of-nodes *times* the total number-of-variables that defines de problem. Each module covers a set of variables. For instance, when incompressible flow is coupled with thermal transport, pressure, velocity and temperature define the problem.
- However, Alya never has the large corresponding matrix system, because the multi-physics solution scheme is a staggered one. For each timestep, the block corresponding to each module is solved sequentially. If required, coupling iterations can be performed to increase accuracy and/or robustness. When more than two modules are coupled, the iterative scheme can be very complex.
- Scalability is measured based on the total time for all the modules as they run in an increasing number of processors. If a module is not properly scaling it will spoil the total performance.

2.2 The parallelization layer

The parallelization paradigm in Alya is a sub-structuring method, using a Master-Worker interaction model between the CPUs. Sub-structuring methods consist essentially in distributing the work among the Workers, letting the Master in charge of simple tasks like I/O. In that sense, most of the iterative solvers implemented in Alya are parallelized classical solvers like GMRES or Conjugate gradient, which convergence do not depend on the number of CPUs. Preconditioners using coarse space corrections (Multigrid, Deflated Conjugate gradient) are implemented independently of the number of CPUs as well. This is not a restriction but a deliberate decision. In fact, if one has tuned a set of parameters to achieve convergence on a given number of CPUs, one would like to obtain the same convergence using

more CPUs. This is a crucial point when considering industrial simulations where the user usually does not necessarily have time to try different sets of parameters depending on the number of available CPUs. Nevertheless, domain decomposition methods like Additive Restricted Schwarz (RAS), Block LU (one block per subdomain), Schur complement solvers, as well as subdomain dependent preconditioners like linelet [13] are also implemented in Alya. These solvers and preconditioners are generally used whenever classical solvers appear not to be robust enough.

2.2.1 Master-Worker strategy

All the details on the parallelization of Alya can be found in papers such as [2, 12, 14], we give here the general idea. The parallelization is based on a Master-Worker strategy. The Master reads the mesh and performs the partition of the element graph with METIS [6], an automatic mesh partitioner which balances the number of elements while minimizing the subdomain boundary/interface surfaces, that is the communications. For the pure MPI strategy, each core will be in charge of each subdomain, which are the workers. The workers build the local matrices (\mathbf{A}_i) and right-hand side (\mathbf{b}_i), and are in charge of the resulting system solution in parallel. In the assembling tasks, very few communications are needed between the workers and the scalability only depends essentially on the load balancing. Basically only few `MPI_AllReduce` are required to compute solution residual, critical time step, etc. In the iterative solvers, the scalability depends not only the load balancing but also on the size of the boundaries between the subdomains and on the communication scheduling.

2.2.2 Communication types and scheduling

In the iterative solvers, two main types of communications are usually needed.

- Global communications via `MPI_AllReduce`, which are used to compute residual norms, time steps and scalar products involved in algebraic solvers;
- Point-to-point communications via `MPI_Isend` and `MPI_Irecv`, which are used in algebraic solvers when sparse matrix-vector (SMV) products are needed.

We mentioned earlier that the parallelization of Alya is based on a sub-structuring approach in which most of the solvers and preconditioners are implemented independently of the number of subdomains. Therefore the parallel solution is, up to round off errors, the same as the sequential one at any moment because mesh partition is only used for distributing work without changing the sequential algorithm. Figure 1 shows these two types of communications in explicit and implicit schemes. The element loop consists of the local (to each subdomain) matrix and RHS assemblies and does not involve communication. Therefore, the parallel performance of the explicit scheme is expected to be dominated by the load balance.

Another key issue of communication is scheduling [15]. Figure 2 shows the kind of problem that can arise when data transfer is not properly scheduled. In this case, four subdomains have to exchange data with all the others. The optimum scheduling is shown on the top part of the figure. On the bottom part, no scheduling is used and subdomains try to exchange their boundary data in a lexical order. In the first communication step, subdomains 3 and 4 cannot send their data to subdomain 1, as this one is being exchanging data with subdomain 2. A bad scheduling can strongly penalize scalability.

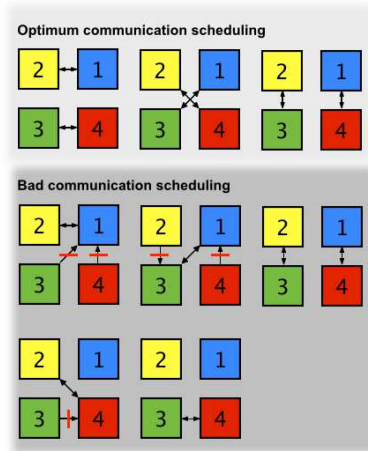


Figure 2: Left: Scheduling strategy on a simple example. Top, optimum and communication scheduling in 3 steps. Bottom, Bad communication scheduling in 5 steps.

2.2.3 Data structure

A specific data structure for distributed memory parallelization has been used and can be briefly explained through a simple example illustrated in Figure 3. It shows an example of mesh partitioning into four subdomains (top left) and its corresponding node numbering (top right). In each slave, interior nodes are first ordered. Then, boundary nodes (grey) are divided into *own boundary nodes* and *others boundary nodes*. The tag *own boundary nodes* cannot be repeated in more than one subdomain and are obtained by partitioning the subdomain boundary with METIS. The *own boundary node* definition is useful when scalar products are needed to avoid repeating the contribution of boundary nodal values. The nodes involved in scalar products are shown in Figure 3 (right) with a \times sign, being 13 nodes in this particular case (bottom left). Finally, the nodes involved in the `MPI_IRecv` and `MPI_Isend` after a SMV are shown (bottom right).

2.2.4 Asynchronous and scheduled SMV

Using the data structure and the scheduling introduced earlier, the Sparse Matrix Vector product is computed together with a non-blocking send-receive as follows:

1. Perform local SVM product $\mathbf{y}_i = \mathbf{A}_i \mathbf{x}_i$ on boundary nodes;
2. Exchange \mathbf{y}_i with neighbors using non-blocking `MPI_Isend` and `MPI_IRecv` according to the communication scheduling;
3. Perform local SVM product $\mathbf{y}_i = \mathbf{A}_i \mathbf{x}_i$ on interior nodes;
4. Synchronize the solution updates with `MPI_WaitAll`.

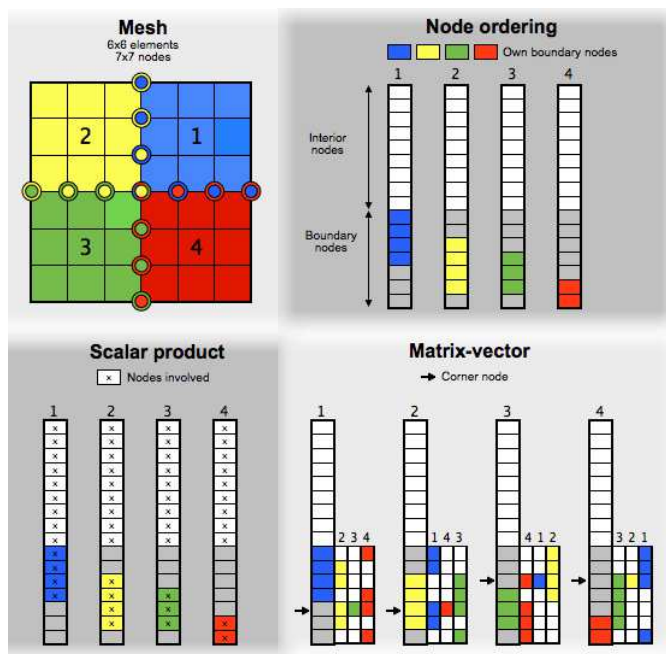


Figure 3: Organization of data in Alya and types of communications.

3 The examples

In this paper we analyze Alya’s parallel behaviour through three different examples:

- The human respiratory system: transient incompressible flow.
- The kiln furnace: transient incompressible flow with a low-Mach approach, heat transport and chemical reactions.
- The electro-mechanical cardiac model: transient non-linear solid mechanics with an hyperelastic model and excitable media.

In all cases we start with meshes in the range of a few million elements, which are progressively subdivided in parallel using the *mesh multiplication* algorithm described in [7], in order to produce large enough meshes to feed a supercomputer up to a hundred thousand cores. Before analyzing the parallel performance, we proceed to briefly describe each of the examples and their associated numerical strategies.

3.1 The respiratory system

Computational simulation enables the mechanics of respiratory airflow to be explored in detail, with considerable potential benefits for healthcare and protection. Resolving the complex time-dependent flow in the large airways poses a severe challenge. Various compromises are generally made, such as restricting the portion of the airways considered and approximating the flow conditions or physics. In this example, the unsteady flow in a

subject-specific model of the domain that extends from the face to the third branch of the bronchopulmonary tree is simulated.

The whole airway geometry was defined from a single subject, identified via retrospective examination of CT images obtained from clinical records at St Marys Hospital, Paddington. Consent was obtained to use this data as the basis for airway segmentation and reconstruction. Segmentation of the airways was performed using the Amira package (TGS Europe) and required some manual intervention, particularly in the nasal airways. There the fine bone structure challenges the resolution typical of data acquired under routine clinical protocols, but the fidelity of the reconstructed data was carefully checked by ENT surgeons. Translation of the coarse segmentation into a smooth surface was performed using in-house, curvature adapted smoothing procedures. Mesh generation was accomplished in stages, using the Gambit and TGrid packages (Ansys Ltd.). This work was done in collaboration with D. Doorly and A. Bates from Imperial College (UK).

The solution of this problem involves the solution of the incompressible Navier-Stokes equations. The time discretization is based on a second order BFD scheme and the linearization is carried out using the Picard method. The space discretization is based on the variational multiscale method (VMS) and is extensively described in [9]. At each time and linearization iteration, the following system

$$\begin{bmatrix} \mathbf{A}_{uu} & \mathbf{A}_{up} \\ \mathbf{A}_{pu} & \mathbf{A}_{pp} \end{bmatrix} \begin{bmatrix} \mathbf{u} \\ \mathbf{p} \end{bmatrix} = \begin{bmatrix} \mathbf{b}_u \\ \mathbf{b}_p \end{bmatrix} \quad (2)$$

is solved, where \mathbf{u} and \mathbf{p} are velocity and pressure nodal unknowns. The direct solution of the system is usually referred to as monolithic scheme. In order to avoid the use of complex preconditioners to account for the velocity-pressure coupling involved in this monolithic system, an algebraic fractional scheme was developed [14]. This scheme enables to segregate the solutions of the velocity and pressure at the algebraic level, by solving the pressure Schur complement using an iterative method (herein the Orthomin(1)). This strategy offers two main advantages. Firstly, with respect to the monolithic scheme, one shot of the method involves the solution of the momentum equation and the solution of a symmetric system for the pressure (Laplacian) representing the continuity equation. The momentum equations usually converge very well, even with a simple diagonal preconditioner. The continuity equation is solved with the Deflated Conjugate Gradient solver (DCG) [12], together with a linelet preconditioner when anisotropic boundary layers [13] are present. Secondly, with respect to classical fractional step methods, no fractional errors are introduced and the solution converges to the same as the monolithic one. What is important to note here is that the solution strategy which consists in solving the pressure Schur complement instead of attacking directly the monolithic scheme, should be understood as part of the algebraic solution strategy of the Navier-Stokes system, and not a fancy trick to escape from this scheme.

Figure 5 shows the strong scalability and efficiency for the respiratory system problem. Scalability is measured comparing the CPU time taken to solve one simulation time step in an increasing number of processors. Efficiency higher than 0.80 is sustained up to 24K processors, where it starts to be degraded due to the higher ratio of communications / computing time. The bars plot at the bottom gives the mean-elements-per-core figure. This

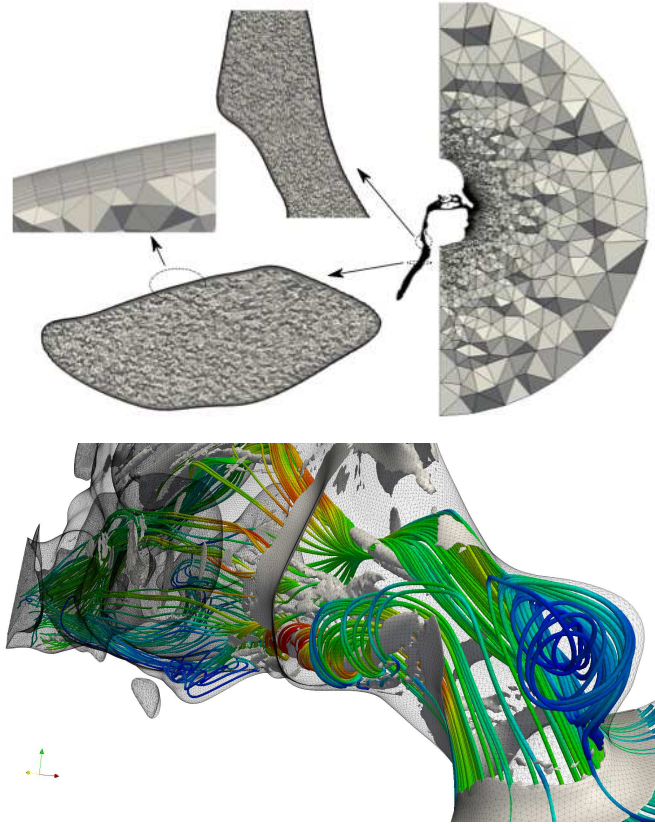


Figure 4: Respiratory system initial mesh (top) and close up view with streamlines.

is very useful to establish a sweet spot, which depending on the problem physics and size, sets the number of processors you need to maintain a high efficiency. If we choose 0.80 as the limit, for this case the sweet spot is around 15.000 elements per core.

3.2 The kiln furnace

At the heart of the cement production process lies the kiln, a tilted rotary oven where raw materials are heated to reaction temperatures to form small pellets called clinker, which is then ground to make cement powder [16]. In addition to reducing its raw material consumption, improving the efficiency of cement kiln is a main concern of the industry, as the kiln is the main consumer of energy in the production process. A kiln is a tilted cylindrical vessel rotating at a fixed frequency of about 5 rpm. Its length ranges between 50 and 180 meters, and its diameter between 2 and 4 meters. On the high part of the kiln the raw material is fed in, sometimes as a dry powder and others as a wet sludge, where it begins the process of clinkerization. On the lower part of the kiln a large burner ejects fuel, typically pulverized coal or waste material. The burner has a primary air injector, and secondary and tertiary injectors that add swirl motion to the flow acting as a flame stabilization mechanism, which

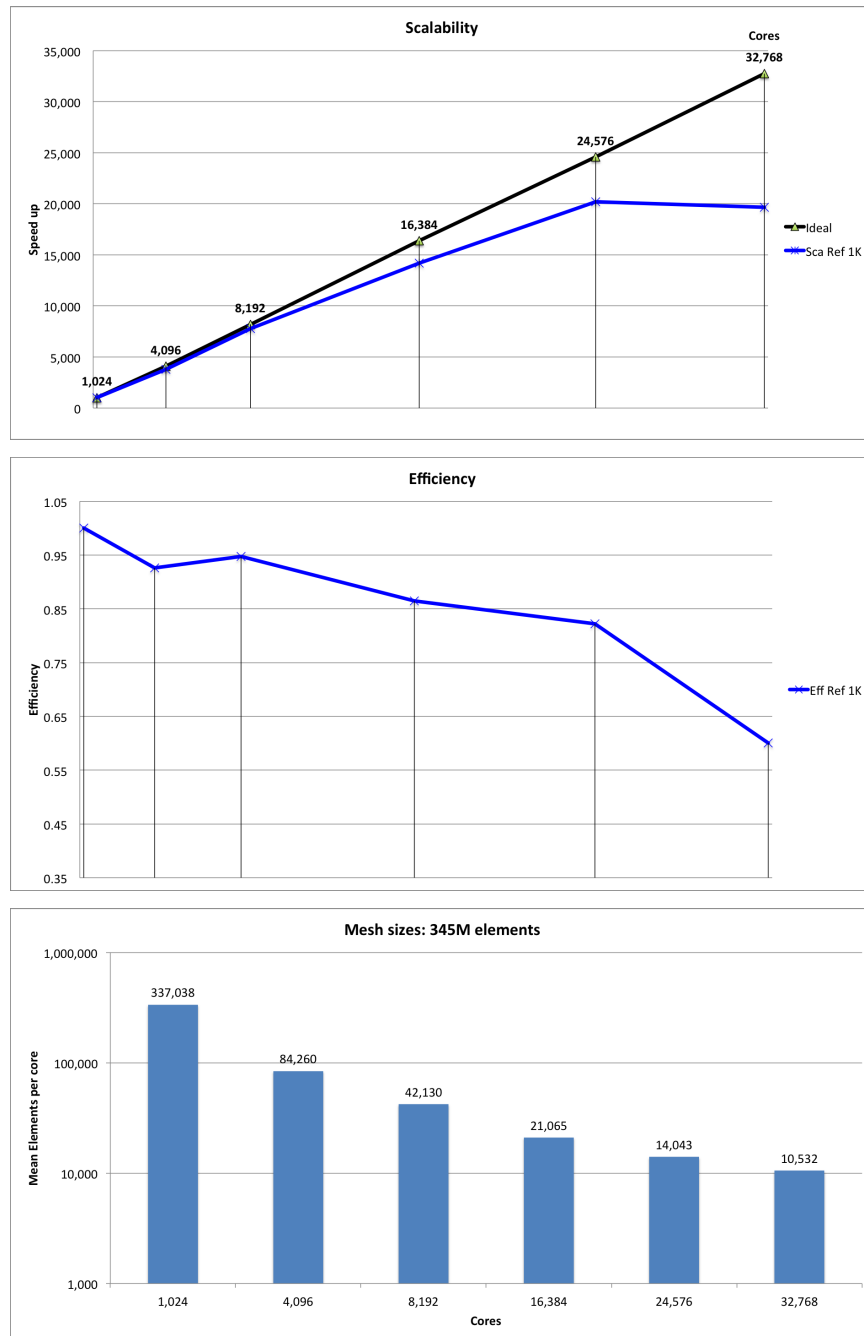


Figure 5: Scalability, efficiency and mean-elements-per-core for the respiratory system simulation.

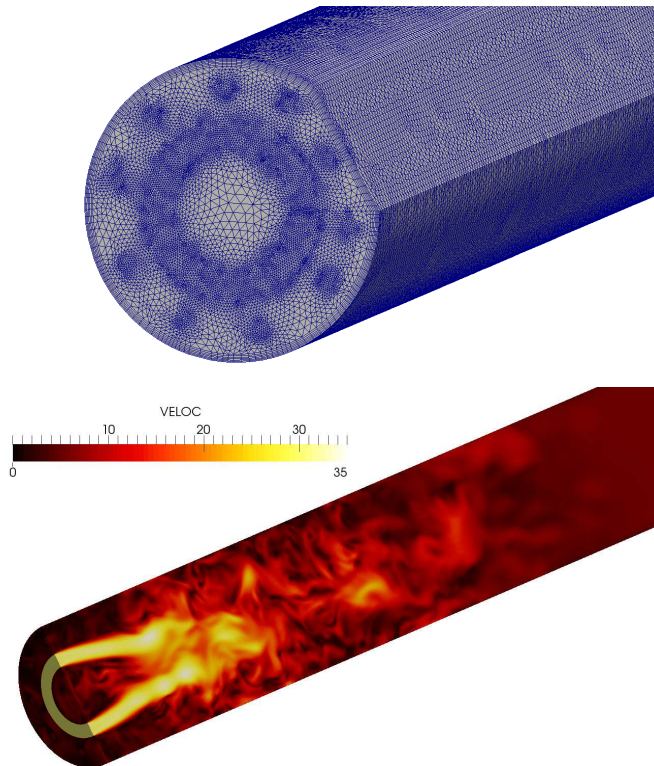


Figure 6: Kiln initial mesh close-up (top) and cut with velocity contours.

can be up to 10 meters long. The walls of the kiln are a mixture of refractory bricks and metal. Furthermore, cement stuck to the walls around the lower third of the oven forms a coating shell critical for operation of the kiln.

In this example, the gaseous phase of a rotary kiln is simulated using large-eddy simulation (LES). The numerical scheme to solve this coupled problem is based on a staggered algorithm that solves the Navier-Stokes equations at the low-Mach limit, the enthalpy transport equation expressed in terms of temperature along with the transport and reaction of the chemical species. In this case, we consider six chemical species to represent the oxidation of methane.

The flow equations are solved using a second order backward difference scheme (BDF) with a Newton-Raphson linearization method. The momentum and continuity equations are solved with unsymmetric and symmetric iterative solvers respectively. For the momentum equations, the GMRES is considered while the Conjugate Gradient (CG) or Deflated CG are the choices for the continuity equation [2, 12]. The GMRES solver is also employed to solve for the enthalpy, turbulence quantities and species mass fractions. The Gauss-Seidel iterative method is employed to solve the species mass fraction until the targeted convergence.

In this problem and following [7], four different levels of mesh subdivision have been considered, referred to here as $h = 1, 1/2, 1/4, 1/8$, from the coarsest to the finest, respectively. The numbers of elements are $8.25M$, $66.0M$, $528M$ and $4.22B$, respectively. The time step

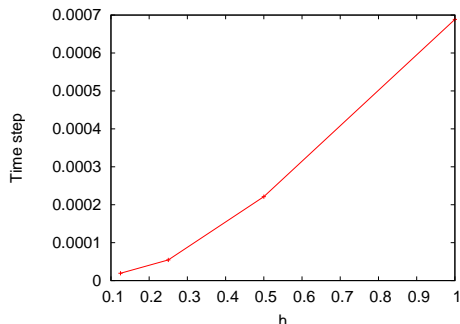


Figure 7: Kiln. Time step values for the four meshes.

size is computed as a multiple of the critical time step. Figure 7 shows the average time step values of the first ten time steps, computed for the four meshes.

Figure 8 shows the strong scalability and efficiency for the kiln example. The plots show the total scalability, measured summing up the CPU times for all the Physical problems solved, namely low Mach, temperature and chemical reactions. In this example we show the results for two meshes: 528M (called DIV2) and 4.22B elements (called DIV3). For DIV2 (labelled “DIV2 Ref 1K”) the scalability is measured all the way from 1024 up to 100K cores, with the sweet spot around 16K mean elements per core. Beyond that point, efficiency falls below 0.80. For DIV3, i.e. the largest mesh, we run the last three points of the plot, 32768, 65536 and 100000 cores, using as the scalability normalizing value the CPU time obtained for 32768 (labelled “DIV3 Ref 32K”). In order to be fair with the comparison, we have added the scalability and efficiency plots for DIV2, but now normalizing with 32768 instead of 1024 (labelled “DIV2 Ref 32K”). As expected, “DIV2 Ref 32K” is very close to a translation upwards of “DIV2 Ref 1K”. On the other hand, “DIV3 Ref 32K” presents a much better scalability and efficiency, with a sustained large efficiency up to 100.000 cores.

Apart from the scalability, we present some convergence results of the solvers of the momentum (GMRES) and continuity equations (DCG). The DCG involves the solution of a coarse problem, using a direct solver, to accelerate the convergence *a la multigrid*, by providing a mechanism to damp out the low frequency errors. In order to keep the number of iterations of the DCG solver constant when refining the mesh, one can increase the number of groups, that is the size of the coarse problem. In the present case, the number of groups is maintained constant and is rather small for the meshes considered (=200). Figure 9 compares the converges of the first iterations for the momentum and continuity equations, using the four meshes. We observe that the momentum equations converge quite rapidly and similarly for the four meshes. This is because the time step decrease with the mesh size, increasing in this way the diagonal terms of the momentum equations, and leaving their condition numbers almost unchanged. This is not the case of the DCG, which converge degrades with the mesh size. However, we observe that even with a very small number of groups, the method still converges. In Figure 10 we plotted the rates of convergence of the GMRES and DCG solvers. These figures can be useful to predict the number of iterations required to achieve a given residual reduction according to the mesh size. In addition, we plotted an approximate linear fit to the rate of convergence of the DCG for this particular case.

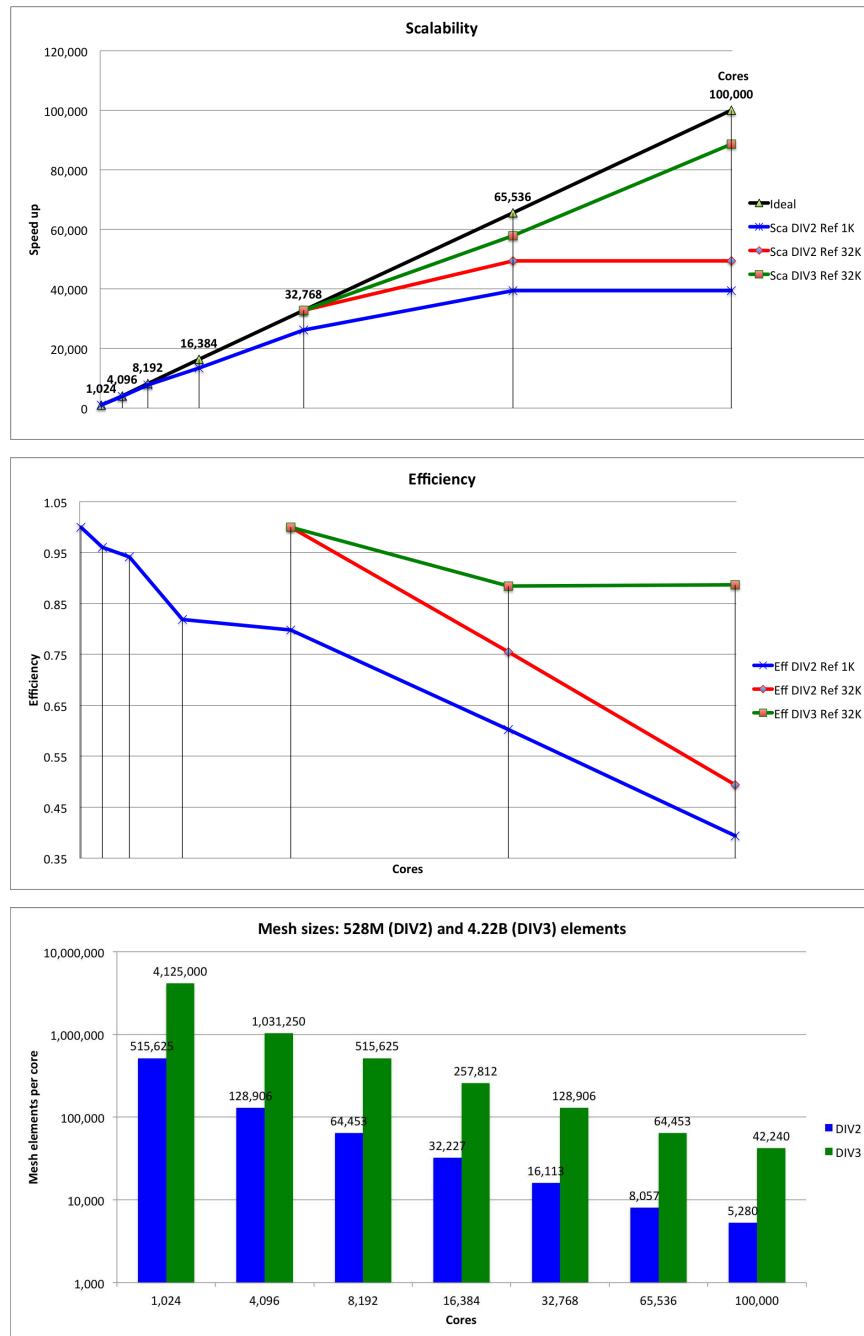


Figure 8: Scalability, efficiency and mean-elements-per-core for the kiln furnace simulation.

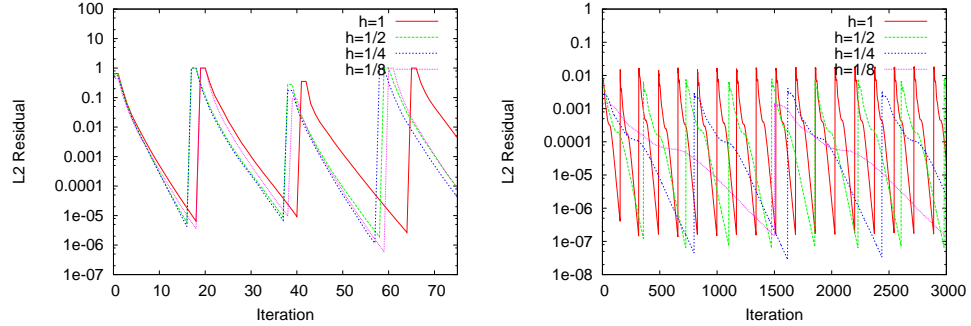


Figure 9: Kiln. Convergence of the momentum (Left) and continuity (Right) equations.

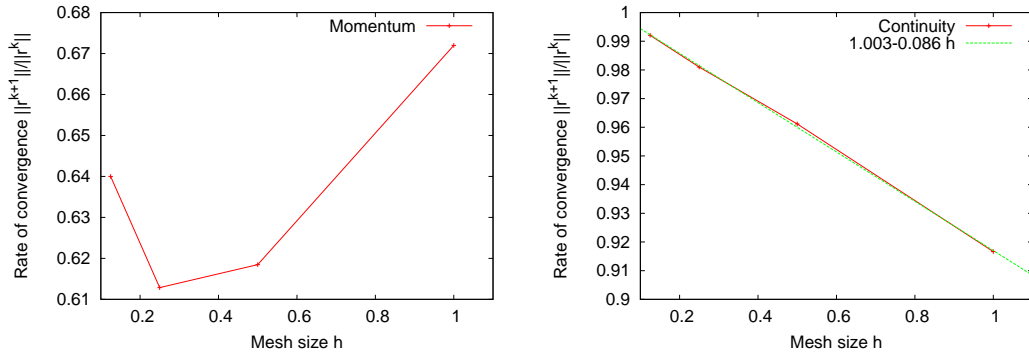


Figure 10: Kiln. rate of convergence of the momentum (Left) and continuity (Right) equations.

3.3 The electromechanical cardiac model

The Alya Cardiac Computational Model is explained in papers such as [5, 17]. Simulating a heart beat is a complex, multiscale problem. This means that many scales are coupled together covering different orders of magnitude: from descriptions of electrical propagation, cells arrangement into a spatial description and up to the geometry of the cardiac chambers [18]. In [19] the authors review the effort to model the behavior of the heart during the last decades, from the molecular point of view to the anatomical level of the organ. On the one hand, electrophysiological models at the cell level consider Ca-based activation. Mechanical models representing the deformation of the tissue are based on protein interaction like actin-myosin and events in cardiac myofilaments and single cells. On the other hand, the electromechanical solution at organ level requires coupling electrical and mechanical components and can include some of the cellular models, depending on the specific application. At the organ-level, the cardiac computational model requires solution of the electrical component as a non-linear reaction-diffusion system, i.e. an excitable media model, the mechanical component, which produces the deformation and a coupling scheme to link both problems together.

The electrical propagation is modelled as a diffusion equation with local anisotropy and a

non-linear term. Anisotropy is due to the fiber-like complex structure of the cardiac muscle, fibers are defined as a nodal field coming from either mathematical modelling or a special kind of Magnetic Resonance Imaging. Combined with the diffusion, the non-linear term produces a sharp depolarization advancing front. In this example, a so-called FitzHugh-Nagumo model is used.

The second Physical problem is the muscular contraction and relaxation. From the mechanical point of view, the myocardium is here considered compressible. The material is hyper-elastic, with anisotropic behaviour ruled by the fiber structure. In this work, we use a transversally isotropic version based on [20] and presented in [5]. The dynamical mechanical equations are written in a total-Lagrangian formulation. The Cauchy stress $\boldsymbol{\sigma} = J^{-1} \mathbf{P} \mathbf{F}^T$, related to the first Piola-Kirchoff P_{iJ} and the deformation gradient $F_{iJ} = \frac{\partial x_i}{\partial X_J}$ and its Jacobian J , allows to define the material model. Stress is developed in two parts: active and passive:

$$\boldsymbol{\sigma} = \boldsymbol{\sigma}_{pas} + \sigma_{act}(\lambda, [Ca^{2+}]) \mathbf{f} \otimes \mathbf{f} \quad (3)$$

The passive part is governed by a transverse isotropic exponential strain energy function $W(b)$ that relates the Cauchy stress $\boldsymbol{\sigma}$ to the right Cauchy-Green deformation b . The passive stress is then

$$J \boldsymbol{\sigma}_{pas} = (a e^{b(I_1-3)} - a) \mathbf{b} + 2a_f (I_4 - 1) e^{b_f(I_4-1)^2} \mathbf{f} \otimes \mathbf{f} + K(J - 1) \mathbf{I} \quad (4)$$

The strain invariant I_1 represents the non-collagenous material while strain invariant I_4 represents the stiffness of the muscle fibers, and a, b, a_f, b_f are parameters to be determined experimentally. K sets the compressibility. Vector \mathbf{f} defines the fiber direction.

Electro-mechanical action depends on ionic concentration in the tissue, being coupling models still under development. The electrical component simulates the propagation of the transmembrane potential by solving a reaction-diffusion system plus some non-linear terms. By solving these equations, ion concentrations ($Ca^{2+}, Na^+, K^+ \dots$) in the cellular membrane can be computed.

Electro-mechanical coupling is modelled as follows. Cardiac mechanical deformation is the result of the active tension generated by the myocytes. The model includes passive and active properties of the myocardium. It assumes that the active stress is produced only in the direction of the fiber and depends on the calcium concentration of the cardiac cell, as described in papers such as [21]:

$$\sigma_{act} = \alpha \frac{[Ca^{2+}]^n}{[Ca^{2+}]^n + C_{50}^n} \sigma_{max} (1 + \beta(\lambda_f - 1)). \quad (5)$$

In this equation, C_{50}^n , σ_{max} and λ_f are model parameters. We have introduced a parameter $0 < \alpha < 1$ to calibrate the amount of active stress and measure its sensitivity.

In order to capture all the required time scales, small time steps are needed. Therefore, in cardiac mechanics simulations explicit schemes for time integration are preferred. Figure 11 shows a snapshot on the electromechanical propagation, closing up on the mesh. The original mesh is made of a bit more than 6M elements. After two and three subdivision cycles following [7], it reaches 427 millions and 3.4 billions tetrahedra respectively.

Figure 8 shows the strong scalability and efficiency for the cardiac electromechanical model. Again, the plots show the total scalability, measured summing up the CPU times

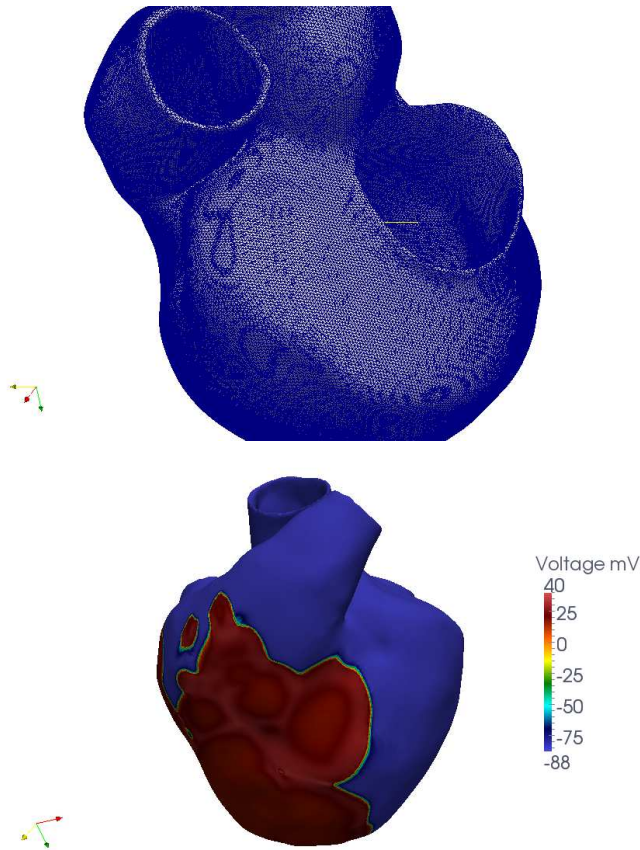


Figure 11: Heart initial mesh (top) and electrophysiology activation potential.

for the Physical problems solved, namely electrophysiology and solid mechanics. As in the kiln example, we show here the results for two meshes: 427M (called DIV2) and 3.416B elements (called DIV3). Using the same approach as above, for DIV2 (labelled “DIV2 Ref 1K”) the scalability is measured all the way from 1024 up to 100K cores. In this case, the sweet spot is lower than 4K elements per core. The reason is that, being the scheme explicit, communication needs per time step are much lower. As in the kiln example, for DIV3, i.e. the largest mesh, we run the last three points of the plot, 32768, 65536 and 100000 cores, using as the scalability normalizing value the CPU time obtained for 32768 (labelled “DIV3 Ref 32K”). We have added the scalability and efficiency plots for DIV2, but now normalizing with 32768 instead of 1024 (labelled “DIV2 Ref 32K”). Again and as expected, “DIV2 Ref 32K” is very close to a translation upwards of “DIV2 Ref 1K”. On the other hand, “DIV3 Ref 32K” presents a much better scalability and efficiency, with a sustained large efficiency up to 100.000 cores.

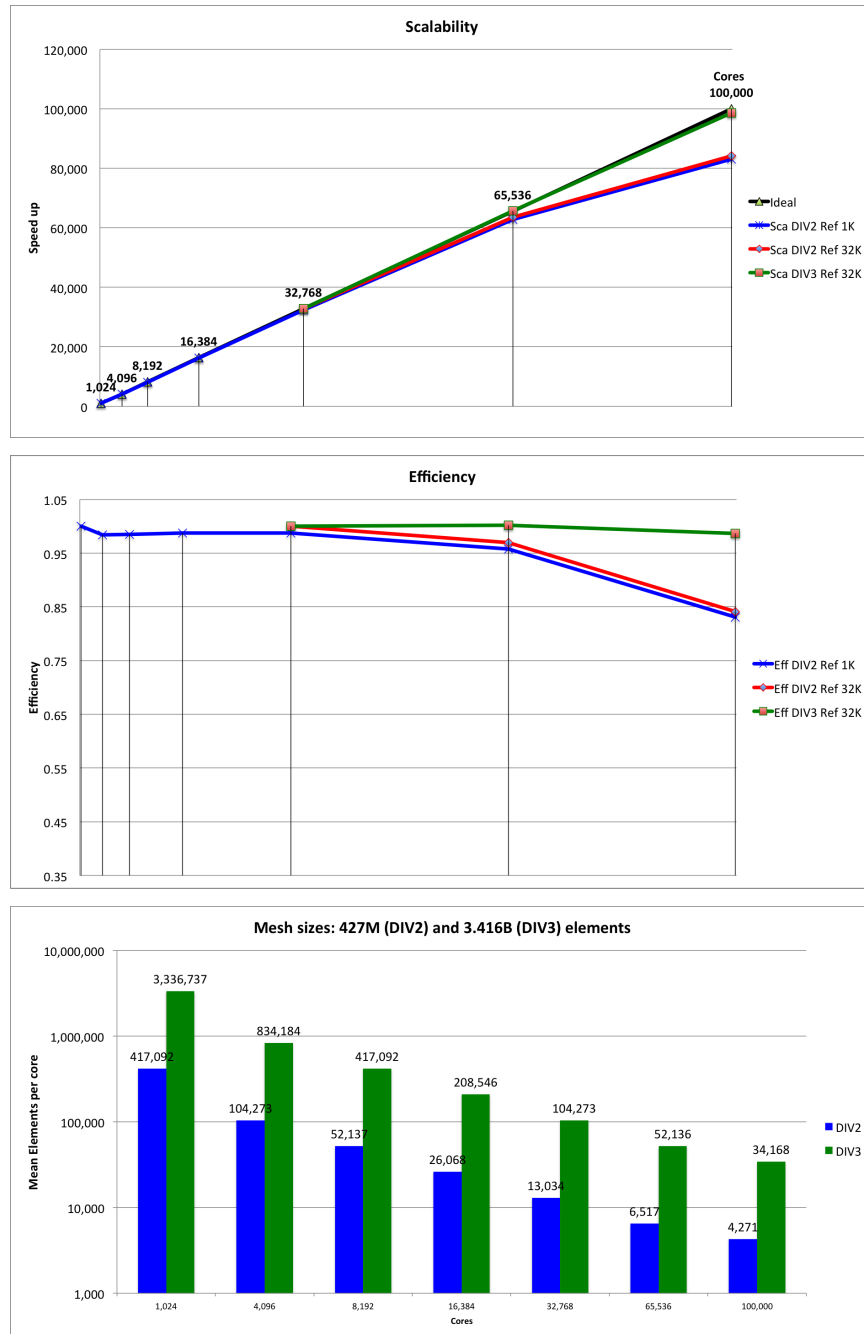


Figure 12: Scalability, efficiency and mean-elements-per-core for the cardiac electro-mechanical simulation.

4 Conclusions and Future Lines

In this paper, we have presented the simulation strategy of Alya, a multi-physics solver designed to run efficiently on tens of thousands of processors, especially well-suited for simulations in the engineering realm. The NCSA's sustained peta-scale system of Blue Waters has shown its potential with large-scale Alya runs maintaining unprecedentedly high parallel efficiency on 100,000 cores, clearly demonstrating the feasibility of petascale (and potentially exascale) computing in engineering.

The chosen examples cover the largest possible range of features such a code should have. We solved coupled multi-physics incompressible fluid mechanics, combustion and thermal flow, non-linear solid mechanics and excitable media. We simulated meshes up to billions of elements. We used both explicit and implicit schemes, showing scalability plots for both cases and analyzing solver convergence for the implicit ones. We used non-structured hybrid meshes combined with a mesh sub-division strategy. Finally, we concluded that very large scale coupled multi-physics simulations are feasible and efficient on tens of thousands of cores when using codes like Alya in systems like Blue Waters.

Such large-scale problems represent a completely new territory, revealing new issues. Solution strategies must be adapted to take advantage of supercomputers. In the case of the Navier-Stokes equations, an algebraic split strategy has enabled us to the use relatively classical iterative solvers with very good convergence and parallel performances for very large unstructured and hybrid meshes. But sufficient load is necessary to keep parallel efficiency as high as possible. The efficiency obtained on some numerical examples gives us some lower bound estimation, depending on the physics and numerical schemes.

Scalability is the first step. Next, solver convergence must be analyzed. We show in this study at what extent Alya strategy is correct, but there are plenty of issues still to be treated. One key problem is postprocessing. For problems of this size, tools such as HDF5 are very important, but their behaviour on these grounds must be analyzed.

The next steps in Alya roadmap towards exascale will take different directions. We will analyze scalability of very large problems, but now when multi-physics are separated, like in the case of Fluid-Structure Interaction. Considering accelerators, let us remark that in recent years, substantial efforts were undertaken to adapt computational sparse methods for evolving GPU systems. We plan to test GPU-based solver and mathematical libraries with Alya such as CuBLAS [22] and Paralution [23] on XK7 nodes of Blue Waters. We also plan to test a massively parallel direct solver library WSMP [24] as a preconditioner for the iterative solvers in Alya. WSMP has shown enough scalability and robustness to perform with multi-million equation problem size on many thousands of cores [25]. Besides, Alya has been tested in Intel Xeon Phi systems with sustained scalability specially using the MPI parallelization paradigm and virtually no effort in porting. Further research in these two lines will be carried out and reported.

Acknowledgment

The authors would like to thank the following fellow researchers and institutions:

- The Private Sector Program at NCSA and the Blue Waters sustained-petascale computing project-supported by the National Science Foundation (award number OCI 07-25070) and the state of Illinois.

- Denis Doorly and Alister Bates (Imperial College London, UK), collaborators of the airways study. Part of this work was financed by European PRACE Type B/C projects.
- The heart geometry was provided by Dr. A. Berruezo (Hospital Clinic de Barcelona) in collaboration with R. Sebastian (UVEG) and O. Camara (UPF), partially financed through project TIN2011-28067 from MINECO, Spain.
- Part of the cardiac model development was financed by the grant SEV-2011-00067 of Severo Ochoa Program, awarded by the Spanish Government.
- Part of the kiln model development was financed by the European Commission in the framework of the FP7 Collaborative project “Advanced Technologies for the Production of Cement and Clean Aggregates from Construction and Demolition Waste (C2CA)”, Grant Agreement No 265189.

References

- [1] “Alya system.” [Online]. Available: <http://www.bsc.es/computer-applications/alya-system>
- [2] G. Houzeaux, M. Vázquez, R. Aubry, and J. Cela, “A massively parallel fractional step solver for incompressible flows,” *J. Comput. Phys.*, vol. 228, no. 17, pp. 6316–6332, 2009.
- [3] G. Houzeaux, R. de la Cruz, H. Owen, and M. Vázquez, “Parallel uniform mesh multiplication applied to a navier-stokes solver,” *Computers & Fluids*, vol. In Press, 2013.
- [4] B. Eguzkitza, G. Houzeaux, R. Aubry, H. Owen, and M. Vázquez, “A parallel coupling strategy for the chimera and domain decomposition methods in computational mechanics,” *Computers & Fluids*, 2013.
- [5] P. Lafortune, R. Arís, M. Vázquez, and G. Houzeaux, “Coupled electromechanical model of the heart: Parallel finite element formulation,” *International Journal for Numerical Methods in Biomedical Engineering*, vol. 28, pp. 72–86, 2012. [Online]. Available: <http://dx.doi.org/10.1002/cnm.1494>
- [6] “Metis, family of multilevel partitioning algorithms.” [Online]. Available: <http://glaros.dtc.umn.edu/gkhome/views/metis>
- [7] G. Houzeaux, R. de la Cruz, H. Owen, and M. Vázquez, “Parallel uniform mesh multiplication applied to a navier-stokes solver,” *Computers and Fluids*, vol. 80, pp. 142–151, 2013.
- [8] “Blue waters-sustained petascale computing system.” [Online]. Available: <https://bluewaters.ncsa.illinois.edu>
- [9] G. Houzeaux and J. Principe, “A variational subgrid scale model for transient incompressible flows,” *Int. J. Comp. Fluid Dyn.*, vol. 22, no. 3, pp. 135–152, 2008.
- [10] Y. Saad, *Iterative Methods for Sparse Linear Systems*. SIAM, 2003.

- [11] Y. Saad, J. Yeung, J. Erhel, and F. Guyomarc'h, "A deflated version of the conjugate gradient algorithm," *SIAM J. Sci. Comput.*, vol. 21, pp. 1909–1926, 2000.
- [12] R. Löhner, F. Mut, J. Cebral, R. Aubry, and G. Houzeaux, "Deflated preconditioned conjugate gradient solvers for the pressure-poisson equation: Extensions and improvements," *Int. J. Numer. Meth. Engn.*, vol. 87, pp. 2–14, 2011.
- [13] O. Soto, R. Löhner, and F. Camelli, "A linelet preconditioner for incompressible flow solvers," *Int. J. Num. Meth. Heat Fluid Flow*, vol. 13, no. 1, pp. 133–147, 2003.
- [14] G. Houzeaux, R. Aubry, and M. Vázquez, "Extension of fractional step techniques for incompressible flows: The preconditioned orthomin(1) for the pressure schur complement," *Computers & Fluids*, vol. 44, pp. 297–313, 2011.
- [15] P. Brucker, *Scheduling Algorithms*, 4th ed. Springer, 2003.
- [16] K. S. Mujumdar and V. V. Ranade, "Simulation of rotary cement kilns using a one-dimensional model," *Chem. Eng. Res. Des.*, vol. 84, pp. 165–177, 2006.
- [17] M. Vázquez, R. Arís, G. Houzeaux, R. Aubry, P. Villar, J. Garcia-Barnós, D. Gil, and F. Carreras, "A massively parallel computational electrophysiology model of the heart," *International Journal for Numerical Methods in Biomedical Engineering*, vol. 27, no. 12, pp. 1911–1929, 2011. [Online]. Available: <http://dx.doi.org/10.1002/cnm.1443>
- [18] I. LeGrice, P. Hunter, A. Young, and B. Smaill, "The architecture of the heart: a data based model," *Phil. Tans. R. Soc. Lond.*, vol. 359, pp. 1217–1232, 2001.
- [19] N. A. Trayanova and J. J. Rice, "Cardiac electromechanical models: from cell to organ," *Frontiers in Computational Physiology and Medicine*, 2011.
- [20] G. A. Holzapfel and R. W. Ogden, "Constitutive modelling of passive myocardium: a structurally based framework for material characterization," *Philosophical Transactions of the Royal Society A: Mathematical, Physical and Engineering Sciences*, 2009.
- [21] S. A. Niederer, P. J. Hunter, and N. P. Smith, "A quantitative analysis of cardiac myocyte relaxation: A simulation study," *Biophysical Journal*, vol. 90, pp. 1697–1722, 2006.
- [22] "Cublas. gpu blas library by nvidia. november 2013." [Online]. Available: <http://docs.nvidia.com/cuda/cublas/index.html>
- [23] "Paralution. paralution-the library for iterative sparse methods on cpu and gpu. november 2013." [Online]. Available: <http://www.paralution.com>
- [24] A. Gupta, "Wsmc : Watson sparse matrix package (part-i: Direct solution of symmetric sparse systems)," IBM T. J. Watson Research Center. Yorkton Heights, NY, Technical Report RC 21866, 2013.
- [25] A. Gupta, S. Koric, and T. George, "Sparse linear solvers on massively parallel machines," in *ACM/IEEE Conference on High Performance Computing SC 2009*, Portland, Oregon, USA November 14-20, 2009.